Lasers in Manufacturing Conference 2021

# Monitoring of the melt pool for fiber laser cutting using a high-speed camera

Max Schleier[a,*], Benedikt Adelmann[a], Cemal Esen[b], Uwe Glatzel[c], Ralf Hellmann[a]

[a]*Applied Laser and Photonics Group, University of Applied Science Aschaffenburg, 63743 Aschaffenburg, Germany*
[b]*Applied Laser Technologies, Ruhr University Bochum, 44801 Bochum, Germany*
[c]*Metals and Alloys, University of Bayreuth, 95447 Bayreuth, Germany*

**Abstract**

We demonstrate an in-situ and coaxial monitoring system based on a high-speed camera with a spectral response in the visible range, which is designed to be integrated into a cutting head between the collimator and processing lens. The thermal radiation from the melt pool is measured in the visible spectral range, without external illumination, spatially and temporally resolved from the top view. The dependencies of the laser power and feed rate on the spectral and geometric information captured from the images of the melt pool in the cut kerf are evaluated. In addition, we developed and show an algorithm to detect incomplete cuts caused by laser power and feed rate from the captured images.

Keywords: In-situ coaxial monitoring; high-speed camera; image processing;

## 1. Introduction

Fiber laser cutting is an established method for cutting metals with different thicknesses. During laser cutting, the material is continuously molten by the focused laser radiation and blown out of the kerf by a gas jet (Mahrle et al., 2009). While laser processing has been comprehensively studied and is widely used, challenges remain for realizing a reliable monitoring system for an in-situ quality control. The high fluid dynamics and complex laser material interaction challenges a successful monitoring and detection of the cut quality (Tenner et al., 2015). One significant influence on cut quality, for laser cutting, is the behavior of the melt flow dynamic on the kerf front (Hirano et al., 2011). With a stable and fast melt flow, good cut qualities

* Corresponding author. Tel.: +49-6022-813692.
*E-mail address:* Max.Schleier@th-ab.de.

are achieved (Arntz et al., 2018). As the feed rate increases, the kerf angle increases, which leads to a higher absorbed irradiation (Lind et al., 2020). Too high temperatures in the kerf cause local vaporization disturbing the melt flow, which in turn results in a deterioration of the cut quality (Bocksrocker et al., 2020).

Therefore, the requirement for a quality controlling monitoring system is the ability to capture the process zone spatially and temporally resolved, in turn demanding for an imaging sensor with high sampling rate. Monitoring approaches for NIR lasers have been reported by Bocksrocker et al., 2015 for coaxial monitoring. Levichev et al., 2020 reported a coaxial monitoring system based on a high-speed camera and demonstrate the correlation between the obtained image and the cut edge quality. Arntz et al., 2019 demonstrate an in situ observation via a trim-cut technique through a transparent substrate for a clear visualization of the melt front inside the kerf.

Against this background, in this proceeding we present a coaxial in-situ high-speed camera (HSC) setup for fiber laser cutting of mild steel sheets, which can be integrated into a cutting head. In this setup, we observe with a HSC the melt flow during a laser cut directly from the top view spatially and temporally resolved in the visible spectral range of the emitted thermal process radiation.

## 2. Methods

### *2.1. Monitoring setup*

Laser cuts are performed with a 4kW multimode fiber laser (IPG Photonics) on mild steel for sheet thicknesses of 1, 3, 5 and 10mm, respectively. Laser and process parameters are summarized in Table 1. To avoid oxidized cutting edges, we use nitrogen as assist gas. The focus position is placed on the bottom of the sheets in all experiments.

Fig 1 schematically depicts the monitoring setup, which is intended to be integrated as an add-on (retrofit) between the collimator and processing lens, consisting of a dichroic mirror, an aperture and a lens for focusing the camera image. The dichroic mirror is designed to reflect the visible spectral part of the thermal process radiation towards the HSC, whereas the wavelength of the fiber laser (1070 nm) and the alignment laser (660 nm) are transmitting. The high-speed recordings are made with a Photron Fastcam Mini AX50, which contains a CMOS with a pixel size of 20 µm x 20 µm and a relative spectral response between 400 – 700 nm. To visualize the thermal radiation, the melt is recorded with 20 000 fps, an image size of 256 x 256 pixels and an exposure time of 1 / 500 000 s.

Table 1. Laser beam and process parameters

| Parameter | Setting |
|---|---|
| Laser Power | 0.5 – 4 kW |
| $M^2$ | 8.5 |
| Fiber core diameter | 100 µm |
| Focus spot diameter | 200 µm |
| Nozzle stand-off | 1 mm |
| Nozzle diameter | 2 mm |
| Nitrogen gas pressure | 8 – 18 bar |
| Feed rate | 5 – 200 mm/s |

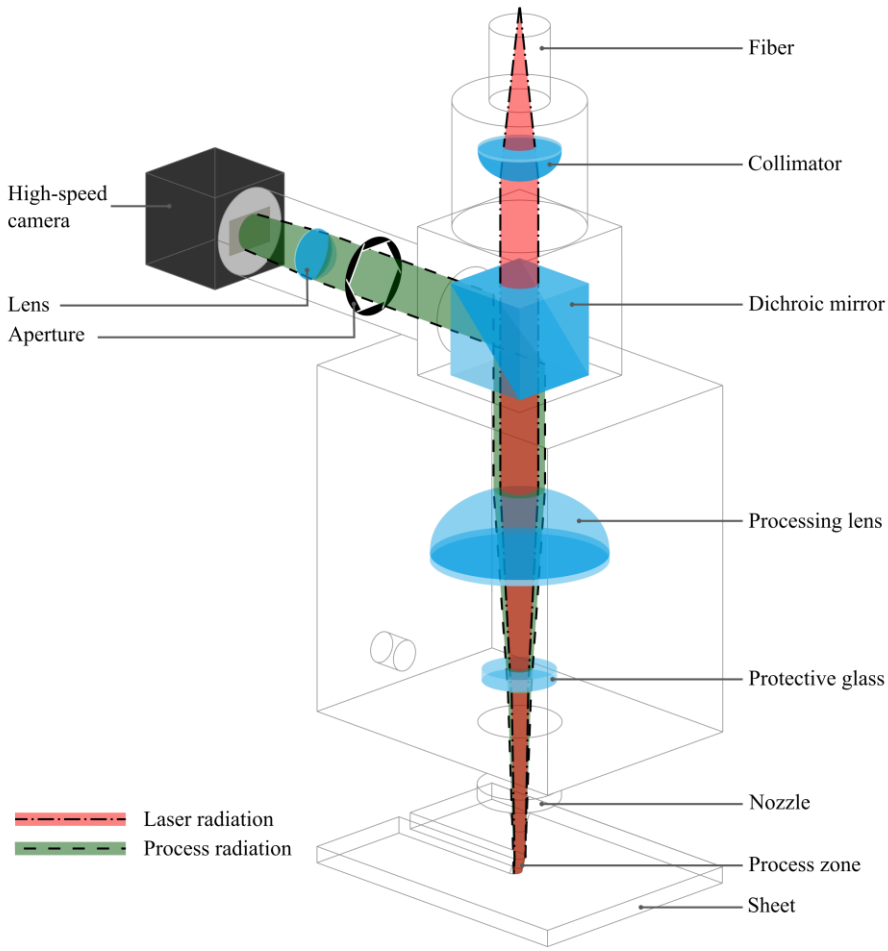


Fig. 1. Illustration of the monitoring setup.

The signal characteristics associated to the melt bath geometry and dynamics of a complete and incomplete cut are enforced by improper cutting parameters. During laser cutting, the emerging thermal process radiation from the melt in the kerf spreads in all direction, partly into the cutting head, where it is collimated by the processing lens. The secondary, thermal process radiation is then reflected by the dichroic mirror and guided to the HSC, where it is recorded.

### *2.2. Evaluation of the HSC images*

To evaluate the cutting process, an initial image analysis calculates spectral and geometrical information from the recorded melt pool in the kerf by a first algorithm, shown in Fig 2. Since the dichroic mirror in the monitoring setup transmits the wavelength of the alignment laser around the wavelength range of 660 nm, nearly no red components are guided towards the high-speed camera. Therefore, only the blue and green components of the visible spectrum from the emitting melt pool are recorded.

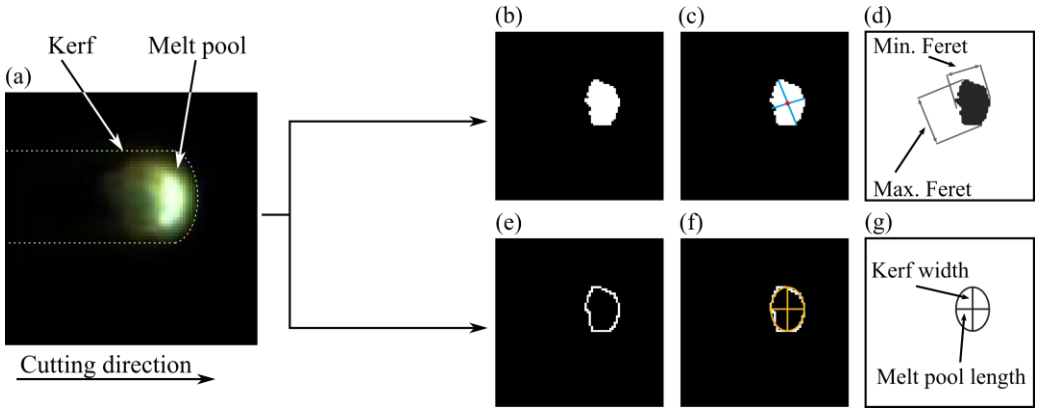


Fig. 2. Illustration of the process of the algorithm, showing the original image (a), the binarized image (b), the feret diameter (c)(d), the edge detection (e) and the calculated ellipse (f)(g).

The color information is digitalized with 8 bit for each color channel, i.e. the intensities for the green and blue channel are available in 256 gradations. In the first step, the area outside of the nozzle's field of view are cut out to reduce the amount of data. Then the image is binarized with a threshold value of 50 for the blue and green channel (cf. Fig 2(a)). The area, center and feret diameter are then calculated from the binarized image. To calculate the area of the melt pool, all white pixels of the binarized image are added up. The feret diameter, which is a measure of objects sizes along specified direction, describes in our image analysis the minimum and maximum distance of the binarized melt pool area. In parallel, the edge of the melt pool is calculated and following an ellipse in the outline of the melt towards the cut front (cf. Fig. 2(f)). The kerf width is calculated from the vertical axis of the ellipse and the melt pool length from the horizontal axis, respectively. Finally, a moving average with a window width of 300 frames (15 ms) is calculated, as individual peaks interfere with the evaluation of further results. In the following examination, we denote the thermal process emission from the green and blue spectral region as green and blue melt pool area.

## 3. Results

Fig 3 summarizes the variation of the melt pool area at the front of the kerf, as determined from the HSC top view images, on laser power, feed rate and sheet thickness, respectively. With increasing laser power and increasing feed rate, the area of the melt increases for all sheet thicknesses on mild steel. The recorded melt pool area increases linearly with increasing laser power, for complete cuts with constant feed rate for a fixed sheet thickness within the tested process window. With improper cutting parameters, a full penetration of the laser beam cannot be achieved and an incomplete cut will occur, resulting in a significant increase of the melt pool area. Parameter regimes leading to such incomplete cuts are shaded grey. A cut is considered as incomplete if the bottom edge of the kerf resolidified. This occurs, e.g., when the laser power is insufficient to pierce through the material or the melt cannot be driven out of the kerf and attached burr seals the bottom side of the kerf.

Fig 4 illustrates the difference between a complete cut with a low and high feed rate and an incomplete. During a complete cut, the metal is molten at the cut front and is driven out of the kerf by the assist gas pressure. The melt emits thermal radiation, depending on the temperature, over a broad spectrum of radiation from the infrared to the UV range. According to Wien's displacement law, the maximum intensity of the spectral specific radiation shifts to shorter wavelength for higher temperatures.

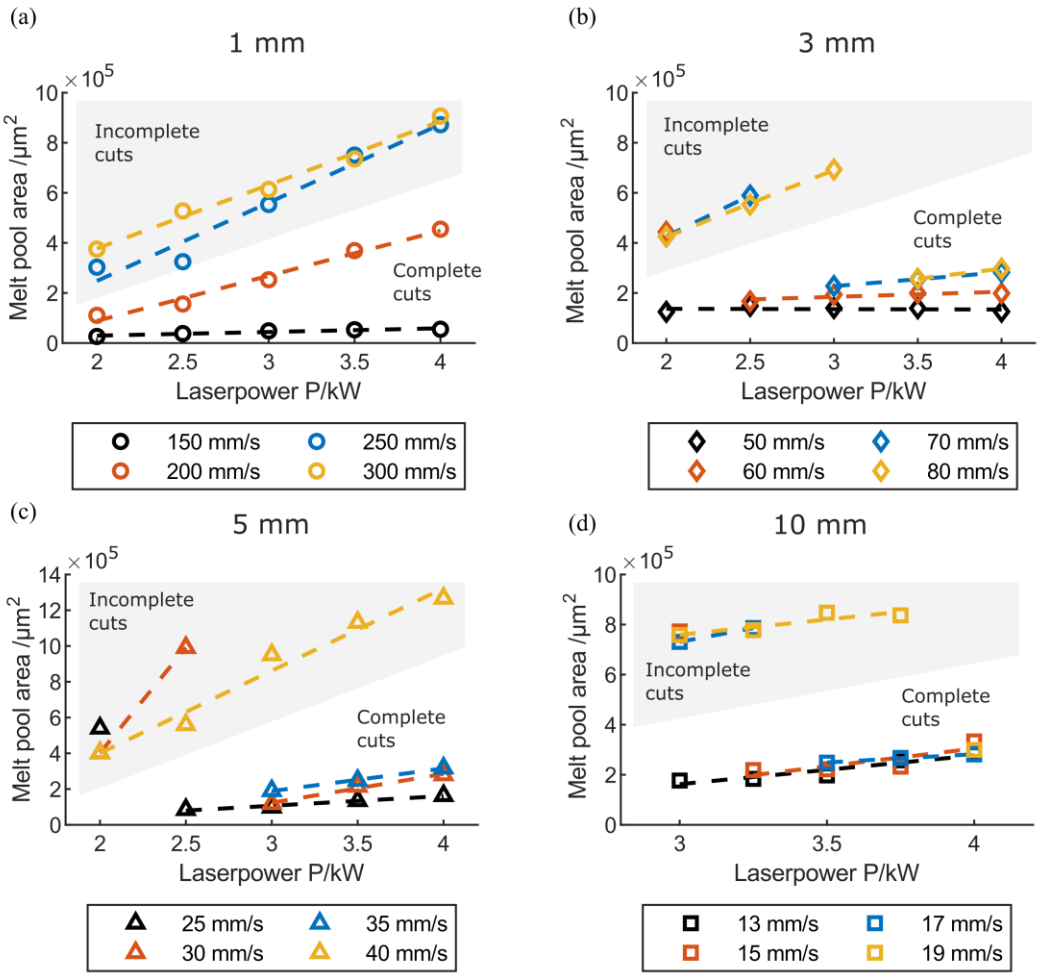


Fig. 3. Average melt pool area for (a) 1 mm, (b) 3 mm, (c) 5 mm, (d) 10 mm thick mild. Incomplete cuts are located in the grey region.

Therefore, the hot areas in the melt pool emit more in the blue spectral range and the little cooler areas thus emit more in the green spectral region. At higher feed rates, the kerf angle increases, which leads to an increased absorption of the laser radiation and thus to a larger melt pool area as captured by the HSC from the top view (cf. Fig 4(d-f)). Fig 4 (g-i) shows an incomplete cut, where the melt is not driven out of the kerf and resolidified. Similar to a complete cut with higher feed rates, the kerf angle for an incomplete cut becomes flatter, increasing the absorbed laser power even more. During incomplete cuts, a plasma plume, which emits in the UV spectral range, may also occur, clearly visible outside of the cutting kerf. However, solely the melt pool area is not sufficient to unambiguously identify a cut interruption, as shown in Fig 3(a) where the same melt pool area is observed for a low laser powers with high feet rate (2 kW, 300 mm/s) and high powers with lower feed rate (4 kW, 200 mm/s). In order to distinguish complete and incomplete cuts, we designed an algorithm based on further characteristic criterion from the spectral and geometric information of the afore described algorithm.

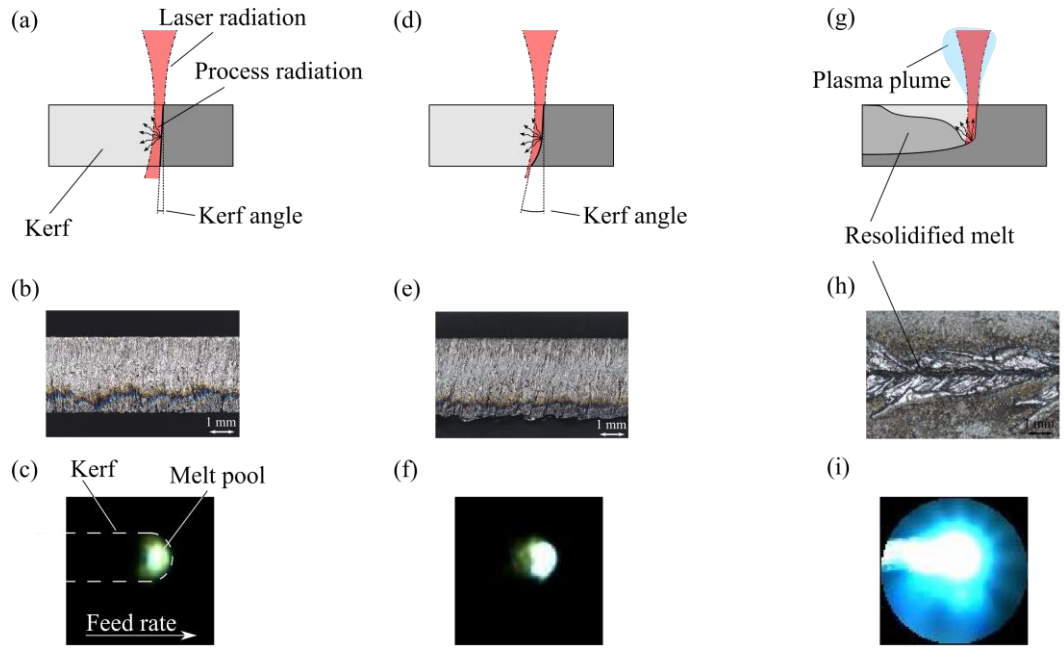


Fig. 4. Illustration of the kerf from the side view during a complete cut (a) with the cut edge (b) and a captured image from the HSC (c) with a slow feet rate, for a complete cut with higher feed rate (d-f) and an incomplete cut with a plasma plume, accordingly with the top view of the sheet (g-h).

Fig 5 shows a flowchart describing the algorithm to identify cut interruptions. In the first step, the melt pool area is checked if it is larger than $6.4 \cdot 10^5$ µm$^2$, defined as an incomplete cut or less than $2.0 \cdot 10^5$ µm$^2$, and defined as a complete cut. This preselection of complete and incomplete cuts is made for cases where the geometries, described from the first algorithm, cannot be calculated, but complete and incomplete cuts clearly occur. This applies to the upper threshold for incomplete cuts, if the melt pool extends over the edge of the nozzle or during the formation of plasma. Respectively to the lower threshold for complete cuts, where the metal is only molten on the cut front and is immediately driven out of the kerf. In the next step, the algorithm probes if the blue melt pool area exceeds 90 % of the green melt pool area. This applies, e.g., during the formation of a plasma, where the size of the blue melt pool area approaches the size of the green melt pool area. Afterwards, it is controlled if the horizontal axis of the ellipse, which represents the melt pool length, exceeds the vertical axis of the ellipse, which represents the kerf width, i.e. the ellipse enlarges in direction of the feed rate. This applies, for incomplete cuts where melt is not driven out downwards and accumulates along the kerf, because of the resolidified bottom edge of the sheet. Further, it is verified if the vertical axis of the ellipse or the minimum and maximum feret diameter pass 98 % of the green melt pool area, which is also assigned to the enlarged melt pool area, duo to higher melt pool temperatures for incomplete cuts with an increased kerf angle and a higher absorbed laser irradiation. Finally, it is checked whether the center of the melt pool area is in the center of the nozzle or shifted in the feed rate direction, since the center of the melt pool also shifts as the ellipse enlarges. The described algorithm detected all 40 incomplete cuts and 88 of 95 complete cuts, which leads to a resulting detection probability of 94 %. This highlights the eligibility of the detection algorithm for use on mild steel in industrial application, as all incomplete cuts were detected that could cause further damage.

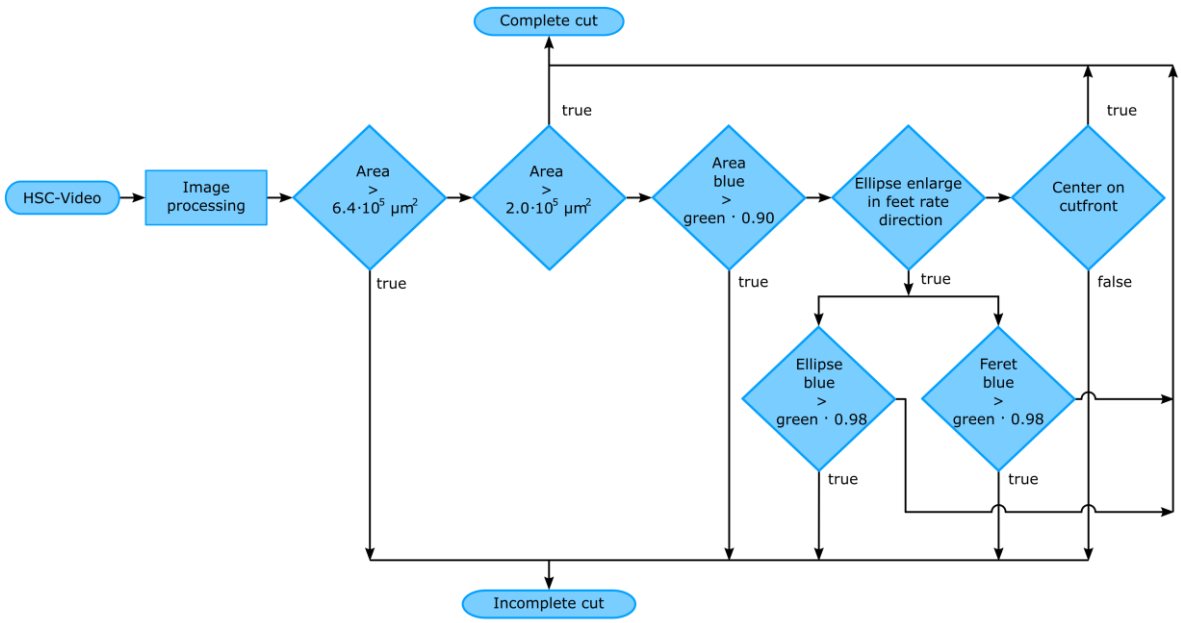


Fig. 5. Flowchart of the detection algorithm for incomplete and complete cuts.

## 4. Summary

We report on a monitoring system based on a high-speed camera with a specifically designed algorithm for image analysis. The detection of cut interruptions is successfully demonstrated for fiber laser fusion cutting of sheet thicknesses between 1 mm to 10 mm. The major advantages of this approach are the wide spectral response and high sampling rate of the camera, paired with high spatial resolution, so the melt pool radiation in the process zone during cutting can be observed coaxially. The dependencies of the laser power and the feed rate on the area of the melt in the kerf from the top view are shown for mild steel. The described algorithm can distinguish between incomplete and complete cuts with a superior detection accuracy of 94 %.

## References

Arntz, D., Petring, D., Schneider, F., Poprawe, R., 2018. In-situ high speed diagnosis--A quantitative analysis of melt flow dynamics inside cutting kerfs during laser fusion cutting with 1 micron wavelength, Journal of Laser Applications 31, p. 022206.

Arntz, D., Petring, D., Stoyanov, S., Quiring, N., Poprawe, R., 2018. Quantitative study of melt flow dynamics inside laser cutting kerfs by in-situ high-speed video-diagnostics, Procedia CIRP 74, pp. 640–644.

Bocksrocker, O., Berger, P., Kessler, S., Hesse, T., Rominger, V., Graf, T., 2020. Local Vaporization at the Cut Front at High Laser Cutting Speeds, Lasers in Manufacturing and Materials Processing 7, pp. 190–206.

Bocksrocker, O., Berger, P., Hesse, T., Boley, M., Graf, T., 2015. „Measurement of the laser cut front geometry“ , 8th Conference Lasers in Manufacturing. Munich, Germany.

Hirano, K., Fabbro, R., 2011. Experimental investigation of hydrodynamics of melt layer during laser cutting of steel, Journal of Physics D: Applied Physics 44, p. 105502.

Levichev, N., Rodrigues, G. C., Vorkov, V., Duflou, J. R., 2021. Coaxial camera-based monitoring of fiber laser cutting of thick plates, Optics & Laser Technology 136, p. 106743.

Lind, J., Fetzer, F., Blazquez-Sanchez, D., Weidensdörfer, J., Weber, R., Graf, T., 2020. Geometry and absorptance of the cutting fronts during laser beam cutting, Journal of Laser Applications 32, p. 032015.

Mahrle, A., Beyer, E., 2009. Theoretical aspects of fibre laser cutting, Journal of Physics D: Applied Physics 42, p. 175507.
Tenner, F., Klämpfl, F., Schmidt, M., 2015. “How fast is fast enough in the monitoring and control of laser welding?”, 8th Conference Lasers in Manufacturing. Munich, Germany.